Acta Crystallographica Section B
Structural Science
ISSN 0108-7681

Polymorphism of $K_2Co_2Mo_3O_{12}$: variations in the packing schemes and changes in molybdenum coordination under high pressure

J. M. Engel,[a]‡ H. Ahsbahs,[b] H. Fuess[a] and H. Ehrenberg[a,c]*

[a]Institute for Materials Science, Darmstadt University of Technology, Petersenstrasse 23, D-64287 Darmstadt, Germany, [b]Institute for Mineralogy, Petrology and Crystallography, Hans-Meerwein-Strasse, D-35032 Marburg, Germany, and [c]Institute for Complex Materials, IFW Dresden, Helmholtzstrasse, 20D-01069 Dresden, Germany

‡ Current address: Technische Universität Dresden, Institut für Werkstoffwissenschaften, Helmholtzstrasse 7, D-01069 Dresden, Germany.

Correspondence e-mail: h.ehrenberg@ifw-dresden.de

Received 12 August 2008
Accepted 18 November 2008

Within systematic studies on the K–Co–Mo–O system so-called high-temperature and high-pressure modifications of $K_2Co_2Mo_3O_{12}$ were found. The Birch–Murnaghan fits for the ambient-conditions modification α (Z = 4) and the high-pressure phase II (Z = 8) lead to V_0 = 1193.09 (4) Å^3, K = 30.8 (8) GPa, K_0' = 5.4 (4) and V_0 = 2170 (10) Å^3, K = 51 (2) GPa with K_0' fixed at 4.0, respectively. The high-pressure phase transition is denoted as pseudoreconstructive [Wiesmann *et al.* (1997). *J. Solid State Chem.* **132**, 88–97], because some [MoO_4] tetrahedra turn into edge-sharing pairs of [MoO_5] pyramids or face-sharing pairs of [MoO_6] octahedra. The new phases are presented and compared with the α phase.

1. Introduction

The investigation of nano-scaled composites is an emerging field in materials science. Their stability, especially over a long timescale and at elevated temperatures, depends crucially on the reaction enthalpies between the components of a composite material. In order to understand stability criteria, or even just to detect the formation of multi-component phases, knowledge of complex phases and their underlying crystal structures is essential. Two examples in the field of quarternary oxides *A*–*T*–*B*–O, where *A* is an alkaline metal, *T* a 3*d* transitional metal and *B* another transition metal with closed electron shells in its ionic form, are given to underline the need for systematic studies of such complex systems:

(i) $LiNiO_2$ and $LiCoO_2$ are used as cathode materials in Li-ion batteries. Their cycle stability is considerably enhanced by coating with ZrO_2 (Miyashiro *et al.*, 2006; Cho *et al.*, 2001). The stability of such composite materials depends strongly on the likeliness of the formation of Li–Ni–Zr–O or Li–Co–Zr–O quarternary phases.

(ii) K_2O is known to promote the catalytic activity of $CoMoO_4$ during the conversion of acetic acid into acetone. However, $K_2Co_2Mo_3O_{12}$ is already formed in this system during calcinations at 623 K for 5 h (Halawy, 2003; Calafat *et al.*, 1998). This phase formation could only be identified, because the existence of this phase and its crystal structure were already known.

The lack of sufficient information on such complex quarternary phases and their stability criteria has initiated our comprehensive investigation of the Na–Fe–Mo–O system (Ehrenberg *et al.*, 2006; Bramnik *et al.*, 2003; Muessig *et al.*, 2003; Muessig, 2004) and is now extended to the K–Co–Mo–O system, where crystalline phases with six different compositions have been found so far (Engel, 2007). All these phases,

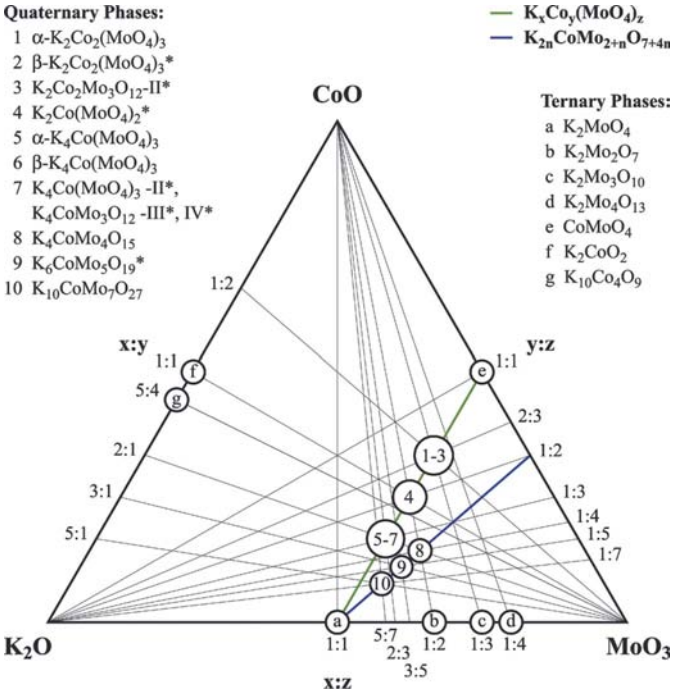

Figure 1
Scheme of phases in the K–Co–Mo–O system (Engel, 2007). Under ambient conditions, all known phases belong to one of two classes, either *ortho*-oxomolybdates with isolated MoO_4 tetrahedra (green line) or members of the $K_{2n}CoMo_{2+n}O_{7+4n}$ family of compounds (blue line), characterized by face-sharing MoO_6 and CoO_6 octahedra, where the members with n = 2, 3 and 5 are known. This figure is in colour in the electronic version of this paper.

which are stable or metastable at ambient pressure, belong either to the group of *ortho*-oxomolybdates $K_xCo_y(MoO_4)_z$ or to the structure family $K_{2n}CoMo_{2+n}O_{7+4n}$ and are summarized in the scheme in Fig. 1 (Gicquel-Mayer & Perez, 1975; Zolotova *et al.*, 1997; Klevtsova *et al.*, 1997; Solodovnikova *et al.*, 1998; Engel *et al.*, 2005). In the *ortho*-oxomolybdates all Mo are exclusively tetrahedrally coordinated, and each O atom belongs to exactly one MoO_4 tetrahedron. In the structure family $K_{2n}CoMo_{2+n}O_{7+4n}$, n = 2, 3 or 5, some of the Mo sites are octahedrally coordinated, and these MoO_6 octahedra share faces with the CoO_6 octahedra. The coexistence of MoO_4 tetrahedra and MoO_6 octahedra at ambient pressure indicates that pressure-induced changes of the Mo coordination might occur in the K–Co–Mo–O system at rather moderate pressures. The progress in the design of diamond–anvil cells for X-ray diffraction (Ahsbahs, 2004) allows the study of pressure-induced phase transitions even for complex oxides. In this contribution we report on three polymorphs of composition $K_2Co_2Mo_3O_{12}$ and discuss the underlying crystal structures with respect to their packing schemes and Mo coordination.

2. Experimental

K_2MoO_4 (Aldrich, 98%/Alfa Aesar 95%), CoO (Alfa Aeser, 99.99%) and MoO_3 (Sigma-Aldrich, 99.5%) were used as educts. In a first step, pure $CoMoO_4$ was prepared from CoO and MoO_3 in a sealed quartz tube, heated up to 1063 K for 120 h. The resulting $CoMoO_4$ was mixed with K_2MoO_4 in an agate mortar in the molar ratio 2:1. The thoroughly ground powder was pressed into a pellet and sealed in a quartz tube. The resulting sample was then kept at 923 K for 72 h. Only reflections from α-$K_2Co_2(MoO_4)_3$ were observed by X-ray powder diffraction, see Fig. 2. In some of the samples individual crystals with another crystal structure but the same composition were found. However, the amount of this β-$K_2Co_2(MoO_4)_3$ phase was too small to be detected by powder diffraction, even in temperature-dependent studies using synchrotron radiation at beamline B2 (Knapp, Baehtz *et al.*, 2004) of HASYLAB in Hamburg, equipped with the position-sensitive detector OBI (Knapp, Joco *et al.*, 2004). The powder data were processed by Rietveld refinement with the *FULLPROF* (Rosinel & Rodriguez-Carvajal, 2001) program package.

For single-crystal X-ray diffraction experiments crystals were

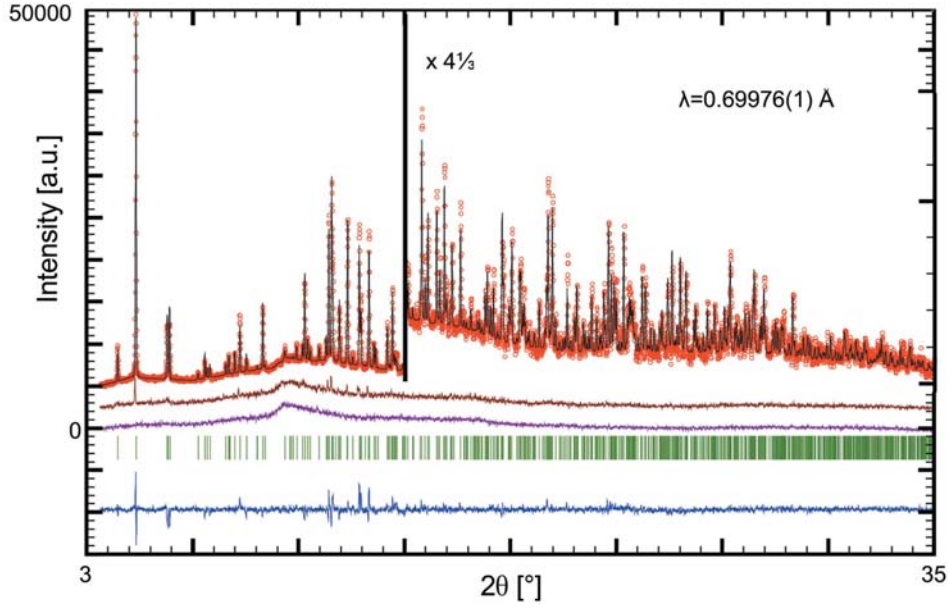

Figure 2
Powder pattern of α-$K_2Co_2(MoO_4)_3$ at 873 K with Rietveld refinement, 973 K (brown curve in the middle) and 983 K (purple curve below, above the vertical reflection marks). The black line shows the corresponding intensities, based on a calculation using Rietveld's method. The blue difference curve between observed and calculated profiles is provided at the bottom below the reflection marks. This figure is in colour in the electronic version of this paper.

Table 1
Crystal data and structure refinement parameters of the phases with the composition $K_2Co_2Mo_3O_{12}$.

	α-$K_2Co_2(MoO_4)_3$	β-$K_2Co_2(MoO_4)_3$	$K_2Co_2Mo_3O_{12})_3$-II
Crystal data			
Chemical formula	$Co_2K_2Mo_3O_{12}$	$Co_2K_2Mo_3O_{12}$	$Co_2K_2Mo_3O_{12}$
M_r	675.88	675.88	675.88
Cell setting, space group	Monoclinic, $P2_1/c$	Monoclinic, $C2/c$	Monoclinic, $P2_1/c$
Temperature (K)	293 (2)	298 (2)	298 (2)
Pressure (GPa)	0.0001	0.0001	9.3 (1)
a, b, c (Å)	7.0093 (1), 8.9624 (2), 19.9977 (4)	7.0418 (3), 19.3329 (7), 17.7267 (7)	13.5237 (8), 7.6440 (4), 18.850 (1)
β (°)	108.247 (2)	97.608 (4)	104.260 (6)
V (Å^3)	1193.09 (4)	2392.04 (16)	1888.58 (18)
Z	4	8	8
D_x (Mg m^{-3})	3.763	3.754	4.754
Radiation type	Mo $K\alpha$	Mo $K\alpha$	Mo $K\alpha$
μ (mm^{-1})	6.59	6.53	8.26
Crystal form, colour	Prism, blue	Needle, blue	Plate, black
Crystal size (mm)	0.14 × 0.11 × 0.06	0.12 × 0.04 × 0.03	0.11 × 0.05 × 0.03
Data collection			
Diffractometer	Xcalibur (TM)†	Xcalibur (TM)†	Xcalibur (TM)†
Data collection method	Rotation‡	Rotation‡	Rotation‡
Absorption correction	Analytical	Analytical	None
T_{min}	0.573	0.509	–
T_{max}	0.751	0.871	–
No. of measured, independent and observed reflections	8014, 2435, 2152	15 336, 3025, 1739	7020, 1154, 791
Criterion for observed reflections	$I > 2\sigma(I)$	$I > 2\sigma(I)$	$I > 2\sigma(I)$
R_{int}	0.017	0.071	0.130
θ_{max} (°)	26.4	29.2	26.0
Refinement			
Refinement on	F^2	F^2	F^2
$R[F^2> 2\sigma(F^2)]$, $wR(F^2)$, S	0.028, 0.137, 1.24	0.038, 0.121, 1.05	0.047, 0.110, 1.05
No. of reflections	2435	3025	1154
No. of parameters	173	178	195
Weighting scheme	$w = 1/[\sigma^2(F_o^2) + (0.098P)^2]$, where $P = (F_o^2 + 2F_c^2)/3$	$w = 1/[\sigma^2(F_o^2) + (0.0529P)^2]$, where $P = (F_o^2 + 2F_c^2)/3$	$w = 1/[\sigma^2(F_o^2) + (0.0538P)^2]$, where $P = (F_o^2 + 2F_c^2)/3$
$(\Delta/\sigma)_{max}$	< 0.0001	< 0.0001	< 0.0001
$\Delta\rho_{max}$, $\Delta\rho_{min}$ (e Å^{-3})	2.94, −1.60	1.76, −1.78	1.07, −0.88
Extinction method	*SHELXL*	None	None
Extinction coefficient	0.0075 (7)	–	–

Computer programs used: *CrysAlis CCD* and *RED* (Oxford Diffraction, 2006), *SHELXS*97, *SHELXS*97, *SHELXL*97 (Sheldrick, 2008), *DIAMOND* (Brandenburg, 2006). † Oxford Diffraction Xcalibur (TM) single-crystal X-ray diffractometer with sapphire CCD detector. ‡ Rotation method: data acquisition using ω and φ scans.

selected under a light microscope. Data acquisition was performed on the Xcalibur system from Oxford Diffraction equipped with a Sapphire 2 CCD detector and the ENHANCE X-ray source option using ω and φ scans. A numerical absorption correction based on the shape of the crystals was applied (Clark & Reid, 1995).

The high-pressure single-crystal X-ray diffraction experiments were performed with three different crystals of α-$K_2Co_2(MoO_4)_3$ using two different diamond–anvil cells (DACs). In the pressure range from 0.5 to 2.7 GPa a Merrill–Bassett DAC with beryllium backpacking, Inconel 718 as the gasket and 2-propanol as the transmitting medium was used (Merrill & Basset, 1974). For the range between 4.9 and 11.7 GPa a 'quadratic' DAC with tungsten gasket and a methanol–ethanol mixture as the transmitting medium, but without any beryllium parts, was used (Ahsbahs, 1995, 2004). Owing to the design of this high-pressure cell, a correction for cell absorption is not necessary.

The pressure in both DACs was determined by the ruby fluorescence method with an accuracy of *ca* ±0.05 GPa. Owing to the tungsten gasket in the 'quadratic' DAC the accuracy is *ca* ± 0.1 GPa as it takes a few days until the pressure is stable after an increase. In this case the pressure during data collection was determined by fitting the pressure *versus* time with a logarithmic fit, see Fig. 3. For the calculation of the parameters of the Birch–Murnaghan equations the *EOSFit*5.2 package was used (Angel, 2000). Diffraction data have been collected in ω and φ scans with the Xcalibur system mentioned above. In the case of the DAC with beryllium the absorption correction was carried out with *Absorb*6.1 (Burnham, 1966; Angel, 2004). Obviously reflections which are not separated have been removed. All crystal structures were solved and refined with *SHELXS* and *SHELXL* (Sheldrick, 2008), respectively.

3. Results

α-$K_2Co_2(MoO_4)_3$ was synthesized as a single phase. In contrast, only very few crystals of β-$K_2Co_2(MoO_4)_3$ were

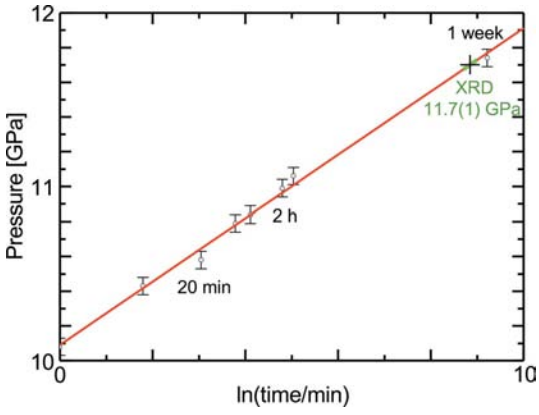

Figure 3
Pressure evolution in the DAC depending on relaxation time. The datapoints are measured by the ruby fluorescence method with corresponding error bars. The red line shows a linear fit, *i.e.* an exponential approach to the saturation value, which allows a very reliable estimation of the actual pressure and its uncertainty in the DAC during the single-crystal X-ray diffraction experiment. This period is marked as the green region. This figure is in colour in the electronic version of this paper.

found in some inhomogeneous reaction products. The crystallographic data for these phases are given in Table 1.[1] The different packing schemes of very similar basic units ($[CoO_6]$ tetramers and $[MoO_4]$ tetrahedra) lead to two different crystal structures with the same number of formula units per asymmetric unit, but a C-centring in the β-phase accompanied by a doubling of the unit-cell volume.

The high-temperature powder diffraction experiments revealed no structural phase transition from α- to β-$K_2Co_2(MoO_4)_3$ due to heating. The diffraction patterns at 873, 973 and 983 K are shown in Fig. 2 as representatives. All observed reflections at 873 K are well explained by the crystal structure of α-$K_2Co_2(MoO_4)_3$. Note that the main differences between observed and calculated patterns are due to changes in the atomic coordinates at elevated temperature, which have been kept fixed from the room-temperature structure and were not refined. The diffraction pattern, recorded at 973 K, shows only weak reflections and at 983 K all the reflections have disappeared, indicating complete melting accompanied by the decomposition of the sample (Klevtsov *et al.*, 1980). Thermal expansion has been analysed in terms of the linear differential thermal expansion tensor (Paufler & Weber, 1999), see Fig. 4.

The new crystal structure type for β-$K_2Co_2(MoO_4)_3$ has also been determined at ambient conditions and has been confirmed by independent analyses of three different crystals. Structure solution and refinement converged to the structure parameters in Table 1, in agreement with the same stoichiometry $K_2Co_2(MoO_4)_3$ as for the α phase. Therefore, this new phase was labelled β-$K_2Co_2(MoO_4)_3$. A comparison of the crystal structures of both polymorphs α and β reveals some common features: In both crystal structures all the Mo ions are tetrahedrally coordinated by oxygen, and all the O atoms belong to the MoO_4 tetrahedron. Therefore, both phases are orthooxomolybdates with isolated MoO_4 tetrahedra. In both crystal structures four CoO_6 octahedra are connected by corner sharing to form tetramers.

The high-pressure single-crystal X-ray diffraction studies on α-$K_2Co_2(MoO_4)_3$ exhibit a phase transition to $K_2Co_2Mo_3O_{12}$-II at *ca* 6.7 GPa with increasing pressure and back to the α phase at *ca* 5.7 GPa during pressure release. This reversible phase transition with hysteresis is accompanied by a colour change of the crystal. Already at *ca* 0.3 GPa the colour of the crystal turns form blue to pink without significant structural changes, while at the phase transition a change from pink to black is observed. All lattice parameters decrease monotonically with increasing pressure (Fig. 5). The lattice parameters of α-$K_2Co_2(MoO_4)_3$ and $K_2Co_2Mo_3O_{12}$-II at different pressures are listed in the supplementary material. The volumes of these two phases at different pressures were fitted with a third-order Birch–Murnaghan equation for the α-phase,

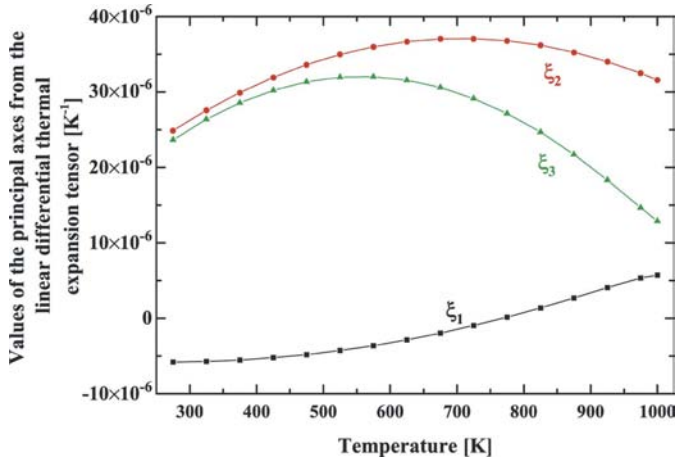

Figure 4
Thermal expansion of α-$K_2Co_2(MoO_4)_3$.

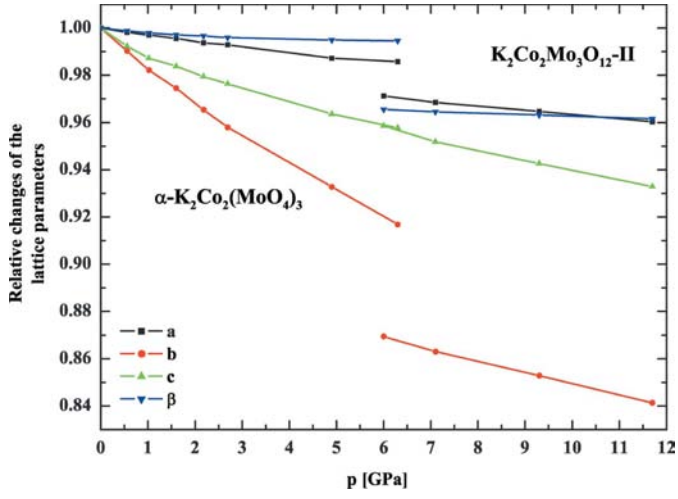

Figure 5
Lattice parameters of α-$K_2Co_2(MoO_4)_3$ and $K_2Co_2Mo_3O_{12}$-II at different pressures, normalized to the initial parameters.

[1] Supplementary data for this paper are available from the IUCr electronic archives (Reference: SN5075). Services for accessing these data are described at the back of the journal.

leading to the parameters V_0 = 1193.09 (4) Å^3, K = 30.8 (8) GPa and K_0' = 5.4 (4) and with fixed K_0' = 4 to V_0 = 2170 (10) Å^3 and K = 51 (2) GPa for the high-pressure phase II. In Fig. 6 experimental data and the corresponding fits are presented for both phases. Furthermore, the crystal structure of $K_2Co_2Mo_3O_{12}$-II was solved and refined. The crystal structure data of $K_2Co_2Mo_3O_{12}$-II at 9.3 (1) GPa are listed in Table 1, the atomic positions provided in the CIF in the supplementary material. The crystal structure of the high-pressure phase reveals coordination changes of some [MoO_4] tetrahedra into pairs of edge-sharing [MoO_5] pyramids and in two face-sharing pairs of [MoO_6] octahedra. The tetramers of CoO_6 octahedra are preserved during the $\alpha \rightarrow$ II phase transition, but the distortions of the octahedra are more pronounced in the high-pressure phase.

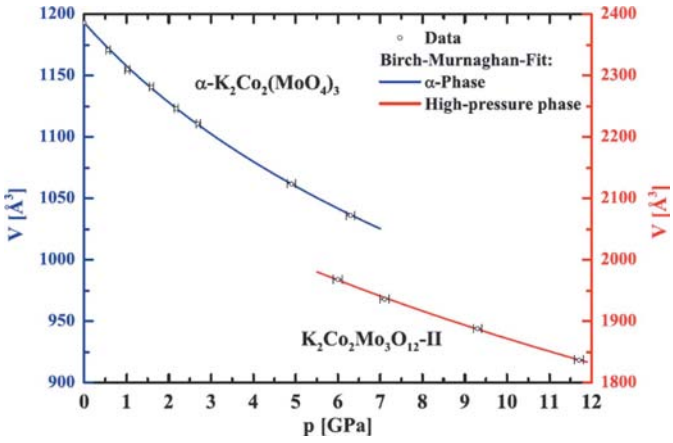

Figure 6
High-pressure data of α-$K_2Co_2(MoO_4)_3$ (blue, upper curve on the left-hand side) and $K_2Co_2Mo_3O_{12}$-II (red, lower curve on the right-hand side) with Birch–Murnaghan fits.

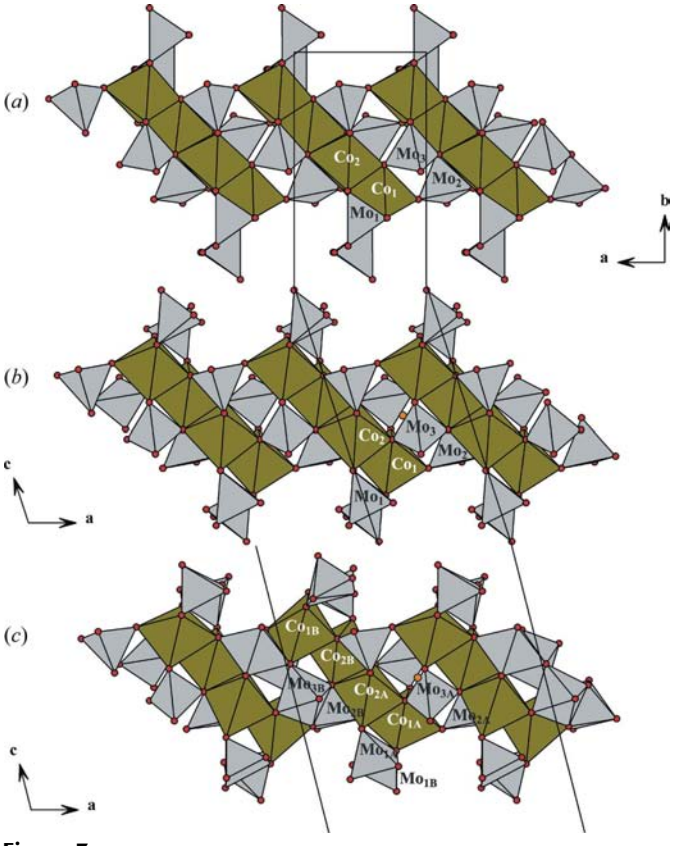

Figure 7
Chains in the crystal structures of: (*a*) β-$K_2Co_2(MoO_4)_3$, (*b*) α-$K_2Co_2(MoO_4)_3$ and (*c*) $K_2Co_2Mo_3O_{12}$-II at 9.3 GPa. [MoO_4] polyhedra, grey; [CoO_6] octahedra, ochre; the inversion centre, orange. The Co and Mo sites in one asymmetric unit are labelled. This figure is in colour in the electronic version of this paper.

4. Discussion

The common feature of all three $K_2Co_2(MoO_4)_3$ polymorphs is tetramers of four edge-sharing [CoO_6] octahedra. All three crystal structures form chains along the *a* axes, built up of the CoO_6 tetramers, linked with each other by Mo—O polyhedra (Fig. 7). The Mo—O polyhedra are exclusively isolated [MoO_4] tetrahedra for the α and β phases, but also corner-sharing pairs of [MoO_5] pyramids and face-sharing pairs of [MoO_6] octahedra in the high-pressure phase −II. The main difference between all three phases is the connectivity scheme for the tetramers and details of the bridging Mo—O polyhedra.

The lattice parameters of all the crystal structures are related with each other and can be expressed in terms of the size of the [CoO_6] tetramer units and their distance from each other. The *c* axis of the α phase and the *b* axis of the β phase scale with the length of two such tetramers, see Figs. 8 and 9, and are therefore very similar. The *c* axis of the β-phase includes two distances between tetramers, but the *b* axis of the α phase only one, reflected in the ratio of the corresponding lattice parameters close to 2:1. The *a* axes in all three phases also scale with the number of tetramer units. In the α and β phases there is one tetramer unit along the *a* axes, but two in the −II phase. Due to compression under high pressure the length of the *a* axis in the −II phase is slightly less than twice

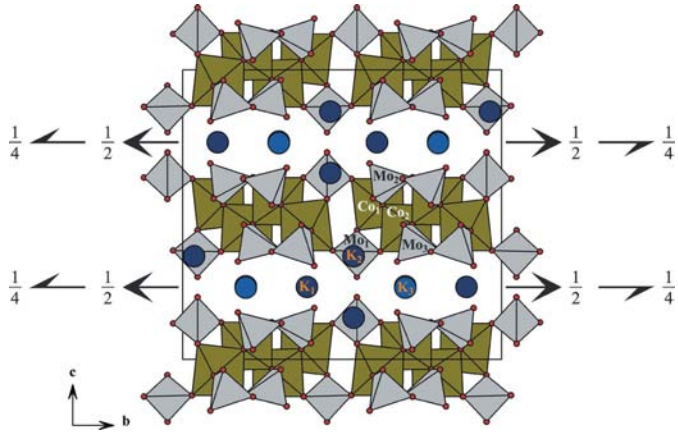

Figure 8
Unit cell of β-$K_2Co_2(MoO_4)_3$ along the *a* axis. The K ions are navy blue and the fractional occupied K sites are a lighter blue. This figure is in colour in the electronic version of this paper.

the value for the other phases. This doubling of the *a* parameter results from the coordination changes in the Mo—O polyhedra, connecting the tetramers to form chains along the *a* axis. In the high-pressure phase two kinds of connectivities are alternating, either exclusively by [MoO_4] tetrahedra or including face-sharing pairs of [MoO_6] octahedra. Beside these coordination changes the *M*—O polyhedra between the chains transform from tetrahedra to pairs of edge-sharing [MoO_5] pyramids (Fig. 10). The pressure-induced phase transition from α-$K_2Co_2(MoO_4)_3$ into $K_2Co_2(MoO_4)_3$-II can be classified as a pseudoreconstructive transition (Wiesmann *et al.*, 1997). On one hand, there is a one-to-one correspondence of all atomic sites in these crystal structures, characteristic for displacive phase transitions. On the other hand, bonds are formed or broken, as typical for reconstructive phase transitions.

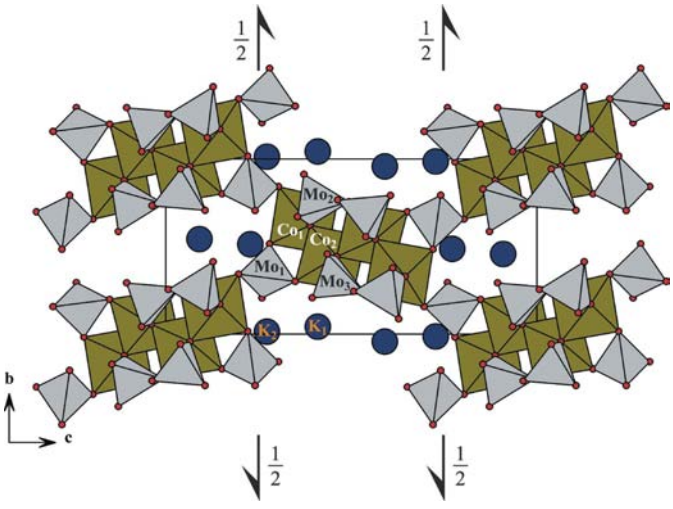

Figure 9
Unit cell of α-$K_2Co_2(MoO_4)_3$ along the *a* axis.

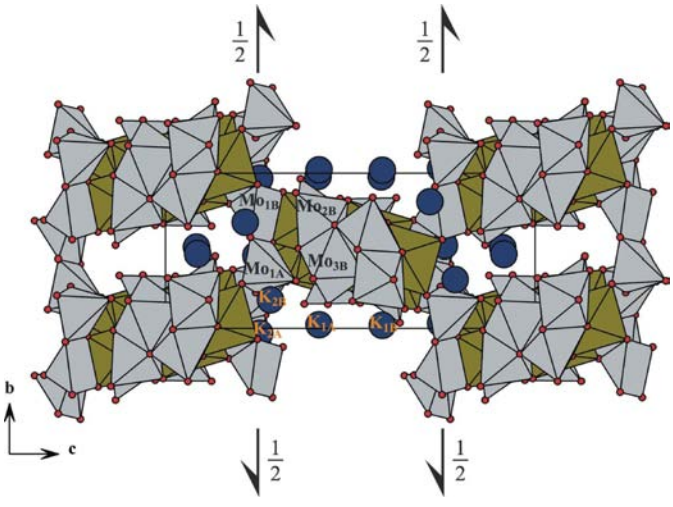

Figure 10
Unit cell of $K_2Co_2Mo_3O_{12}$-II along the *a* axis.

The conditions for the formation of β-$K_2Co_2(MoO_4)_3$ remain unclear. This phase is formed under quenching conditions and remains metastable in some exceptional cases. However, it cannot be completely ruled out that this phase is stabilized by a small excess or deficiency in K corresponding to a slight deviation from the site-occupation factor s.o.f = $\frac{1}{2}$ for the K3 site. As all known phases in the K–Co–Mo–O system (prepared under similar conditions with respect to partial oxygen pressure) are in agreement with an assignment of Co^{2+} and Mo^{6+}, the exact composition of $K_2Co_2(MoO_4)_3$ also seems to be more likely for the β phase. Note that a s.o.f. < $\frac{1}{2}$ for K3 would require a higher oxidation state than +2 for some Co ions or oxygen deficiencies, while a s.o.f. > $\frac{1}{2}$ means a lower oxidation state than +6 for some of the Mo ions. The phase was proposed as a high-temperature phase, because of some structural changes with respect to the α phase, which are characteristic for high-temperature phases: first, the splitting of K sites into distinguishable but not fully occupied sites. A second criterion was the increasing symmetry from primitive to C-centred monoclinic. However, a detailed analysis of the symmetries challenges the latter argument, because one more atomic parameter, $y(K_3)$, is needed for the β phase than for the α-phase to define the crystal structure model completely. In this sense the monoclinc C-centred crystal structure of the β phase with $Z = 8$ is of lower symmetry than the primitive monoclinic one with $Z = 4$ for the α phase. In spite of similar structural features, the transformation from the α to the β phase requires a breaking of the connectivity between the chains and a collective rotation of half of its units. Such a reconstructive phase transition is very likely to be kinetically hindered. The absence of a temperature-induced $\alpha \leftrightarrow \beta$ transformation may thus be explained.

Financial support from the Deutsche Forschungsgemeinschaft (DFG) under grant No. EH183/2 and by the Bundesministerium für Bildung und Forschung (BMBF) under grant No. 05KS7OD2 are gratefully acknowledged.

References

Ahsbahs, H. (1995). *Z. Kristallogr.* Suppl. 9, 22.
Ahsbahs, H. (2004). *Z. Kristallogr.* **219**, 305–308.
Angel, R. J. (2000). *Rev. Mineral. Geochem.* **41**, 35–60.
Angel, R. J. (2004). *J. Appl. Cryst.* **37**, 486–492.
Bramnik, K. G., Muessig, E. & Ehrenberg, H. (2003). *J. Solid State Chem.* **176**, 192–197.
Brandenburg, K. (2006). *DIAMOND*. Crystal Impact GbR, Bonn, Germany.
Burnham, C. W. (1966). *Am. Mineral.* **51**, 159–167.
Calafat, A., Vivas, F. & Brito, J. L. (1998). *Appl. Catal. A*, **172**, 217–224.
Cho, J., Kim, T. J., Kim, Y. J. & Park, B. (2001). *Electrochem. Solid State Lett.* **4**, A159–A161.
Clark, R. C. & Reid, J. S. (1995). *Acta Cryst.* A**51**, 887–897.
Ehrenberg, H., Muessig, E., Bramnik, K. G., Kampe, P. & Hansen, T. (2006). *Solid State Sci.* **8**, 813–820.
Engel, J. M. (2007). PhD thesis. Faculty of Materials and Earth Sciences, Darmstadt University of Technology.
Engel, J. M., Ehrenberg, H. & Fuess, H. (2005). *Acta Cryst.* C**61**, i111–i112.

Gicquel-Mayer, C. & Perez, G. (1975). *Rev. Chim. Miner.* **12**, 537–545.
Halawy, S. A. (2003). *MHC*, **134**, 371–380.
Klevtsov, P. V., Kim, V. G. & Klevtsova, R. F. (1980). *Sov. Phys. Crystallogr.* **25**, 175–180.
Klevtsova, R. F., Glinskaya, L. A., Solodovnikova, Z. A., Zolotova, E. S., Klevtsov, P. V. & Solodovnikov, S. F. (1997). *J. Struct. Chem.* **38**, 426–433.
Knapp, M., Baehtz, C., Ehrenberg, H. & Fuess, H. (2004). *J. Synchrotron Rad.* **11**, 328–334.
Knapp, M., Joco, V., Baehtz, C., Brecht, H. H., Berghaeuser, A., Ehrenberg, H., von Seggern, H. & Fuess, H. (2004). *Nucl. Instrum. Methods Phys. Res. A*, **521**, 565–570.
Merrill, L. & Basset, W. A. (1974). *Rev. Sci. Instrum.* **45**, 290–294.
Miyashiro, H., Yamanaka, A., Tabuchi, M., Seki, S., Nakayama, M., Ohno, Y., Kobayashi, Y., Mita, Y. & Usami, A. (2006). *J. Electrochem. Soc.* **153**, A348–A353.
Muessig, E. (2004). PhD thesis. Faculty of Materials and Earth Sciences, Darmstadt University of Technology, http://elib.tu-darmstadt.de/diss/000514/.
Muessig, E., Bramnik, K. G. & Ehrenberg, H. (2003). *Acta Cryst.* B**59**, 611–616.
Oxford Diffraction (2006). *CrysAlis CCD* and *CrysAlis RED*. Version 1.171.31.4. Oxford Diffraction Ltd, Abingdon, Oxfordshire, England.
Paufler, P. & Weber, T. (1999). *Eur. J. Mineral.* **11**, 721–730.
Rosinel, T. & Rodriguez-Carvajal, J. (2001). *Eur. Powder Diffr.* **7**, 118–123.
Sheldrick, G. M. (2008). *Acta Cryst.* A**64**, 112–122.
Solodovnikova, Z. A., Glinskaya, L. A., Klevtsova, R. F., Klevtsov, P. V. & Solodovnikov, S. F. (1998). *J. Struct. Chem.* **39**, 230–237.
Wiesmann, M., Ehrenberg, H., Miehe, G., Peun, T., Weitzel, H. & Fuess, H. (1997). *J. Solid State Chem.* **132**, 88–97.
Zolotova, E. S., Solodovnikova, Z. A. & Solodovnikov, S. F. (1997). *J. Struct. Chem.* **38**, 83–88.